Structure Structural insights into the allosteric activation of the LicT antiterminator by PTS- mediated phosphorylation -

Yinshan Yang, André Padilla, Karine de Guillen, Léa Mammri, Jérôme Gracy, Nathalie Declerck, Héléne Démèné

Structure

Structural insights into the allosteric activation of the LicT antiterminator by PTS-mediated phosphorylation

--Manuscript Draft--

Manuscript Number:	STRUCTURE-D-18-00254R
Full Title:	Structural insights into the allosteric activation of the LicT antiterminator by PTS-mediated phosphorylation
Article Type:	Short Article
Keywords:	transcriptional antiterminator; NMR; carbohydrate catabolism; phosphorylation; Phosphomimetic mutations
Corresponding Author:	helene demene Montpellier, FRANCE
First Author:	Yinshan Yang, Dr
Order of Authors:	Yinshan Yang, Dr
	André Padilla, Dr
	Léa Mammri
	de Guillen Karine, Dr
	Jérome Gracy, Dr
	Nathalie Declerck, Dr
	Hélène Déméné, Dr
Abstract:	LicT belongs to an essential family of bacterial transcriptional antitermination proteins controlling the expression of sugar-metabolizing operons. When activated, they bind to nascent mRNAs, preventing premature arrest of transcription. The RNA-binding capacity of the N-terminal domain CAT is controlled by phosphorylations of two homologous regulation modules by the phosphotransferase system (PTS). Previous studies on truncated and mutant proteins provided partial insight into the mechanism of signal transduction between the effector and regulatory modules. We report here the conformational and functional investigation on the allosteric activation of full-length LicT. Combining fluorescence anisotropy and NMR, we find a tight correlation between LicT RNA binding capacity and CAT closure upon PTS-mediated phosphorylation and phosphomimetic mutations. Our study highlights fine structural differences between activation processes. Furthermore, the NMR study of full-length proteins points to the back and forth propagation of structural restraints from the RNA binding to the distal regulatory module.

Centre de Biochimie Structurale
CNRS-INSERM-UM1

Dr. Hélène Déméné
Tel : + 33 (0) 467 41 77 01
Fax : +33 (0) 467 79 13
e-mail : Helene.Demene@cbs.cnrs.fr

To Andrej Sali
Academic Editor,
Structure

Montpellier, October the 18th.

Dear Dr. Sali

We would like to thank you for considering our manuscript " Structural elucidation of the allosteric activation of LicT antiterminator by PTS-mediated phosphorylation" (STRUCTURE-D-18-00254R) for publication. We have

- uploaded the Supplemental data as a PDF file,
- resized the graphical abstract to the appropriate size
- eliminate all "first" statements
- provided the Lead contact name and coordinates, with an agreement statement in the Key resource section,
- included two missing references (Pons et al. 1996; Tina et al. 2011) in the reference list,
- corrected the software name from Tina to PIC (Key resource table), corrected the PDB code of CAT structure to 1L1C,
- specified that we have generated 3D models of activated LicT and native LicT in the Key resource table
- corrected the term "asterics" to asterisk" in the supplemental file.

Thank you again for your consideration,

Sincerely yours,

Dr. Hélène Déméné.

Dr. Hélène Déméné
Tel : + 33 (0) 467 41 77 01
Fax : +33 (0) 467 79 13
e-mail : Helene.Demene@cbs.cnrs.fr

To Andrej Sali
Academic Editor,
Structure

Montpellier, October the 18th.

Dear Dr. Sali

We would like to thank you for considering our manuscript " Structural elucidation of the allosteric activation of LicT antiterminator by PTS-mediated phosphorylation" (STRUCTURE-D-18-00254R) for publication. We have

- uploaded the Supplemental data as a PDF file,
- resized the graphical abstract to the appropriate size
- eliminate all "first" statements
- provided the Lead contact name and coordinates, with an agreement statement in the Key resource section,
- included two missing references (Pons et al. 1996; Tina et al. 2011) in the reference list,
- corrected the software name from Tina to PIC (Key resource table), corrected the PDB code of CAT structure to 1L1C,
- specified that we have generated 3D models of activated LicT and native LicT in the Key resource table
- corrected the term "asterics" to asterisk" in the supplemental file.

Thank you again for your consideration,

Sincerely yours,

Dr. Hélène Déméné.

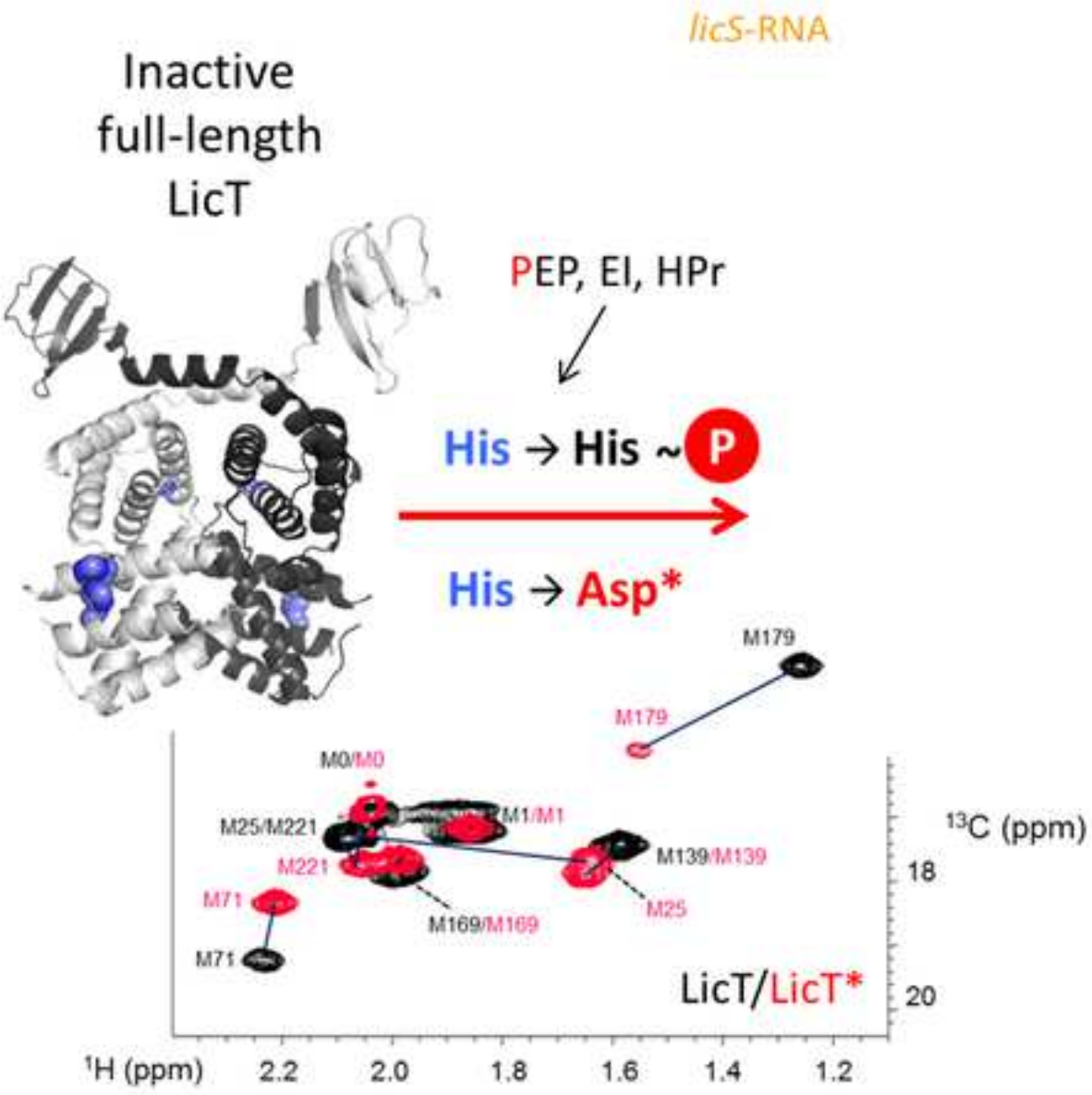

Structural insights into of the allosteric activation of the LicT antiterminator by PTS-mediated phosphorylation.

Yinshan Yang[1], André Padilla[1], Karine de Guillen[1], Léa Mammri[1], Jérome Gracy[1], Nathalie Declerck[1,2,*], Hélène Déméné[1,3*]

[1]Centre de Biochimie Structrurale (CBS), INSERM, CNRS, Univ Montpellier, 29 rue de Navacelles, 34090 Montpellier, France.

[2]INRA, MICA department, 78352 Jouy-en-Josas, France

[3]Lead contact: Hélène Déméné

*Corresponding authors: Hélène Déméné (Helene.Demene@cbs.cnrs.fr) and Nathalie Declerck (Nathalie.declerck@cbs.cnrs.fr)

Summary

LicT belongs to an essential family of bacterial transcriptional antitermination proteins controlling the expression of sugar-metabolizing operons. When activated, they bind to nascent mRNAs, preventing premature arrest of transcription. The RNA-binding capacity of the N-terminal domain CAT is controlled by phosphorylations of two homologous regulation modules by the phosphotransferase system (PTS). Previous studies on truncated and mutant proteins provided partial insight into the mechanism of signal transduction between the effector and regulatory modules. We report here the conformational and functional investigation on the allosteric activation of full-length LicT. Combining fluorescence anisotropy and NMR, we find a tight correlation between LicT RNA binding capacity and CAT closure upon PTS-mediated phosphorylation and phosphomimetic mutations. Our study highlights fine structural differences between activation processes. Furthermore, the NMR study of full-length proteins points to the back and forth propagation of structural restraints from the RNA binding to the distal regulatory module.

Keywords: BglG-like antitermination protein; NMR; phosphohistidine; LicT; Phosphomimetic mutations;

Introduction

Transcriptional antiterminators of the BglG family represent a widespread family of bacterial regulators controlling carbohydrate catabolism in response to the external medium composition (Deutscher et al., 2006; Rutberg, 1997; Stülke et al., 1998). They participate to the metabolic status of the cell and are connected with various cellular processes, such as biofilm formation or pathogen virulence (Görke and Stülke, 2008; Galinier and Deutscher, 2017). They are controlled by the phosphoenolpyruvate (PEP)-dependent sugar phosphotransferase system (PTS) via an interplay of reversible phosphorylations (Deutscher et al., 2006; Postma et al., 1993; Tortosa et al., 2001a). *Bacillus subtilis* LicT represents a prototypical BglG-type antiterminator in Gram positive bacteria. It controls the expression of the *bglPH* operon and of the *licS* gene involved in the uptake and degradation of complex sugars such as aryl-β-glucosides. In its activated state, LicT binds to nascent mRNA at a short palindromic ribonucleic antiterminator (RAT) sequence overlapping a regulatory transcriptional terminator upstream of *bglP* and *licS* (Tortosa et al., 2001a). LicT binding stabilizes the stem-loop structure adopted by the RAT and prevents the formation of a competing terminator hairpin that otherwise promotes transcription arrest (Ait-Bara et al., 2017; Clerte et al., 2013).

LicT and homologous antitermination proteins are composed of three modules (Figure 1A): a short N-terminal RNA binding module (CAT), and two homologous PTS regulatory modules (PRD1 and PRD2). The isolated CAT domain is constitutively active. In the full-length protein, RNA binding is governed by reversible phosphorylations on PRD1 and PRD2 histidine residues by the PTS in response to the presence of specific sugars. Briefly, a phosphate group is transferred successively from PEP to the general PTS components, enzyme I (EI) and HPr, which in turn phosphorylate the β-glucoside transporter (EII^{bgl}) that inactivates LicT by phosphorylation on the conserved H100 and H159 histidines in PRD1 (Bahr et al., 2011; Tortosa et al., 2001a). In the presence of β-glucoside, the incoming sugar is the preferred final acceptor of the phosphorylation chain, and LicT PRD1 remains unphosphorylated. To reach full activity, LicT also requires phosphorylation by HPr on the conserved histidines H207 and H269 in PRD2. This phosphorylation occurs in the absence of glucose or other

preferred carbohydrates and relieves LicT from catabolite repression (Görke and Stülke, 2008; Tortosa et al., 2001a). Initial studies on BglG, the LicT homolog in *E. coli*, suggested that its activation relies on a monomer-dimer switch (Amster-Choder and Wright, 1992). For LicT, the best characterized member of this family, the structural study of single and bi-module fragments suggested a different view of the activation process (Figure 1A). The NMR structure of the isolated CAT module revealed a homodimeric structure that remains unchanged upon the binding of one RNA molecule, resulting in a complex of 2:1 stoichiometry (Yang et al., 2002). Crystallographic studies of PRD1-PRD2 fragments, either native or bearing phosphomimetic mutations, showed homodimers in a compact and open configuration respectively (Graille et al., 2005; van Tilbeurgh et al., 2001). A panel of low-resolution structural studies (X-Ray scattering, analytical ultra-centrifugation, surface plasmon resonance) also revealed extensive remodeling of the dimeric interface leading to dimer stabilization upon activation (Declerck et al., 2001). Our NMR study of two protein fragments, composed of a CAT and a PRD1 domain, one in the native state (CAT-PRD1) and the other in an activated mutant state (CAT-PRD1* carrying the D99N mutation) suggested a regulation model where signal transduction between the CAT and PRD modules is mediated by a structural change in the CAT-PRD1 linker (Déméné et al., 2008). This linker folds as a helix in the native state, opening the dimeric interface of CAT, whereas its loose structure in mutant CAT-PRD1* enables CAT closing and RNA binding. The linker of the CAT-PRD1 bi-module from the GlcT antiterminator also adopts an helix fold (Himmel et al., 2012a) in the crystallized monomer. We used LicT fragment structures to build models of the full-length native and activated forms (Figure 1B). However, the validity of these models is challenged by the reductionist approach based on fragment and mutant proteins.

We present here the structural insights into the activation pathway of full-length LicT by phosphorylation and activating mutations. We combined NMR and fluorescence anisotropy to characterize native (inactive) LicT, PTS-phosphorylated LicT (LicT-P) and the phosphomimetic mutant LicT-H207D/H269D (LicT*), where the PTS-targeted histidines of the PRD2 module have been mutated to aspartic acid. Our work establishes that LicT activation relies on massive rearrangements at the dimeric interface that enables closing of the CAT module, otherwise resting in an open configuration in its native state. Our study also highlights some differences between previous approaches based on

protein fragments and protein mutants and enables a comparative analysis between the RNA complexes formed by native LicT and activated LicT*.

Results

Activating mutations induce CAT closure as seen by ^{1}H NMR.

Our previous study (Déméné et al., 2008) suggested that the D99N-activating mutation in PRD1 in the CAT-PRD1* fragment caused the closure of the CAT domain into a RNA-binding competent motif (Figure 1B). We used ^{1}H NMR to investigate the structural impact of phosphomimetic mutations in PRD2 in the full length protein. The protons of V23 methyl group have a characteristic high-field shifted resonance at -0.4 ppm in the closed structure of CAT, due to the ring-current effect of F48 aromatic side-chain in the other protomer (Figure 2A). This resonance was retrieved in the spectra of active CAT-PRD1* and LicT*, but not of CAT-PRD1 nor full length LicT, suggesting that the PRD2 phosphomimetic mutations caused CAT closure in LicT*.

^{1}H-^{15}N correlation spectroscopy highlights similarities and differences between fragments and full length proteins.

We then further investigated the structural states of the active and inactive full-length proteins by ^{1}H-^{15}N NMR spectroscopy. The linewidths of active LicT* ^{1}H-^{15}N HMQC correlation peaks were narrow and compatible with a unique conformational state (Figure 2B). The correlation time of 21 ns estimated from 1D ^{15}N-^{1}H TRACT experiments (Lee et al., 2006) indeed corresponded to the expected molecular weight of the protein (Figure S1A). By contrast, the inactive protein exhibited correlation peaks with broad linewidths (Figure 2C), compatible with several populations of interconverting substates at a µs-ms timescale. In our previous study (Déméné et al., 2008), we identified an ensemble of eight CAT residues (I7, N8, N10, S13, E22, G26, G28 and F48) that exhibited low-field shifted proton resonances, and can serve as markers of CAT closure. The "closed" fingerprint of CAT was conserved in the full-length activated mutant LicT*, as opposed to native, inactive LicT (Figures 2B, 2C).

A measure of the structural discrepancy $D_{i/j}$ between two proteins i and j is the cumulative sum of the difference between the chemical shifts of their residues. We used this index, calculated from the

chemical shifts of this eight residues ensemble, to quantify CAT similarities among the different constructs (Figure S1B). This index confirmed that CAT closed and open architectures were conserved across the active (CAT, CAT-PRD1* and LicT*) and inactive (CAT-PRD1 and LicT) states respectively. However, all $D_{i/j}$ values were above the error threshold (estimated at 0.015 ppm), establishing that the conservation was not perfect. According to this index, CAT configuration in the active state is the most different between CAT and LicT*, whereas it is more conserved between CAT and CAT-PRD1* on one side, and CAT-PRD1* and activated LicT* on the other side (Figure S1C).

By contrast, ^{1}H-^{15}N correlation peaks corresponding to residues in the PRD modules superposed perfectly in LicT* and PRD1-PRD2* spectra (Figure 2D), showing that the backbone structure of the regulatory domains is identical in the full-length and CAT-truncated mutant proteins. Despite a certain resemblance, the poor quality of the spectra recorded for native LicT and PRD1-PRD2 precluded a similar conclusion for the inactive state (Figure 2E).

^{13}C methionine labelling provides activation markers for each LicT module

We sought to simplify the NMR spectra of the full-length proteins by using ^{13}C-methionine labelling. Assignment of the methionine correlation peaks for LicT and LicT* full-length forms was achieved by extension of the assignment obtained for the protein fragments (Figure S2). All methionine peaks could be unambiguously assigned, but those of M25 and M221 of LicT which lie in close vicinity (^{1}H 2.06/2.09 ^{13}C 17.08/17.13). Figures 2E and 2F establish that five correlation peaks were markedly different between LicT and mutant LicT*, namely M25 (CAT), M71 (PRD1), M139 (PRD1), M179 (PRD2) and M221 (PRD2), three of them belonging to the dimer interface (M25, M71, and M221) (Fig. 1B). At the concentrations of the NMR study (here 200 μM), both proteins are dimeric and the observed differences are thus due to surface remodeling of dimeric surface in three functional modules. These methionine peaks thus represent conformational probes of the dimeric configuration of their respective domain. In addition, the better quality of ^{1}H-^{13}C correlation spectra (compared to ^{1}H-^{15}N spectra) retrieved for LicT and PRD1-PRD2 confirmed that the inactive states of regulatory modules are similar between the full-length protein and the CAT-truncated construct (Figure 2G).

RNA binding by LicT upon activation by phosphomimetic mutation and PTS-mediated phosphorylation

We next wanted to elucidate the structural mechanism of LicT activation by phosphorylation. We thus undertook the functional and structural characterization of full-length LicT after *in vitro* phosphorylation in the presence of PEP and the general PTS components EI and HPr from *B. subtilis*. Previous studies combining P^{32} radioactive incorporation and mass spectrometry established that among the 8 histidines of LicT, the PTS enzymes phosphorylated the conserved ones, namely H100, H159, H207 and H269 (Lindner et al., 1999, Tortosa et al., 2001). H207 and H269 were found to be the major sites of EI/HPr-dependent phosphorylation. Here we also proceeded to a mass spectrometry analysis of LicT and LicT* before and after phosphorylation with non-radioactive PEP. Although these analyses were hampered by endogenous phosphorylations on non-conserved histidines, they confirmed the appearance of peptides phosphorylated at the conserved histidines with the *B. subtilis* PTS enzymes (Figure S3).

We then quantified the protein interactions with the LicT cognate *licS*-RAT antiterminator RNA (Figure S4A) by fluorescence anisotropy experiments (Figure 3A and Table 1). An important increase in RNA binding was observed after incubation of LicT with the phosphorylating enzymes, the dissociation constant (Kd) estimated from the titration curves dropping from 93 ± 21 nM to 6.8 ± 4.3 nM. However, the RNA binding capacity of LicT after phosphorylation (LicT-P) did not reach that of the phosphomimetic mutant LicT* (Kd of 1.7 ± 0.6 nM), indicating that LicT-P was not fully equivalent to LicT*. No change in the RNA binding of LicT* was observed upon incubation with the PTS enzymes (LicT*-P), in agreement with the constitutive activation reported *in vivo* for this mutant protein (Tortosa et al. 2001).

Conformational changes upon phosphomimetic mutation and PTS-mediated phosphorylation

We then investigated on LicT conformational changes induced by phosphorylation *versus* phosphomimetic mutations. As previously observed (Declerck et al., 2001), analytical size exclusion chromatography (SEC) revealed different elution profiles for native LicT and mutant LicT* (Figure 3B). The molecular weights (MW) retrieved from multi-angle light scattering analysis of the SEC profiles confirmed that LicT* is present as a stable dimer (estimated MW of 68.2 +/- 2.9 kDa for an expected MW of 67.8 kDa) while LicT skewed elution peak, centered around 58 kDa and extending down to 40 kDa, points to a monomer/dimer transition (Figure S4B). The elution profiles are in line with the

respective Kd of 0.2 and 2 μM for monomer/dimer equilibrium of activated and native protein which were previously estimated by analytical ultracentrifugation (Declerck et al., 2001).The elution profile of LicT*-P was identical to that of LicT*, whereas that of LicT-P revealed two peaks, corresponding to the LicT* dimer and to the monomer/dimer peak observed before phosphorylation, respectively (Figure 3B). These data show that PTS-mediated phosphorylation of LicT stabilizes the active dimeric configuration. Comparison of the protein fluorescence emission spectra (Figure S4C) also suggested the appearance of LicT dimers in the active conformation after phosphorylation. Accordingly, the ^{1}H NMR spectrum of LicT-P displayed a peak at -0.4 ppm corresponding to the chemical shift of V23 methyl groups in CAT closed structure (Figure 3C). In contrast, no change was observed for LicT* under the same phosphorylation conditions.

Conformational changes were investigated in more details by NMR experiments on ^{13}C-CH_3-ε-Met-labelled LicT (Figure 3D and 3E). Phosphorylation shifted the correlation peaks of the dimerization markers M25 (CAT) and M71 (PRD1), to the positions observed for activated LicT* (^{1}H 1.62/^{13}C 17.39 ppm and ^{1}H 2.21/^{13}C 18.45 ppm respectively), whereas the correlation peaks of the PRD2 dimerization markers M179 and M221 disappeared. Repeating phosphorylation at a higher concentration of LicT (300 versus 80 μM) (Figures S4D-E) showed that the absence of these two peaks was not due to a concentration issue, but more likely related to conformational exchange in PRD2. This differential behavior of PRD2 dimerization markers hints to differences in the dynamics of this regulatory module between the phosphomimetic mutation and the enzymatic phosphorylation.

RNA binding impacts the conformation and/or dynamics of the distal regulatory PRD2 module

Finally, we investigated how RNA binding impacted LicT structure. The solution structure of LicT RNA-binding domain in complex with *licS*-RAT had revealed how the symmetrical CAT dimer recognizes the two asymmetric internal loops of the antiterminator hairpin (Figure 4A) (Yang et al., 2002). This asymmetry induced the doubling of most NMR resonances of CAT residues. In order to minimize the complexity of the NMR spectra, we designed a quasi-symmetric RNA target, named *sym*-RAT, predicted to fold as a hairpin with two identical internal loops (Figure 4B). Although the affinity for this RNA probe was decreased by about two orders of magnitude compared to that for *licS*-RAT, the

relative strengths of the interactions with the different LicT constructs were respected (Figure 4C and Table 1).

Complexation of *sym*-RAT to LicT* (Figure 4D) at 100 µM caused minor shifts in ^{1}H-^{13}C methionine correlation peaks, showing that RNA-binding does not induce major structural changes, as was reported for isolated CAT (Yang et al., 2002). The most impacted residue was M25, whose correlation peak apparently merged with the adjacent correlation peak of M139. In addition, the correlation peak of M179, from the PRD2 module, whose intensity was initially low, almost disappeared. To further investigate this point, we measured the methionine relative peak intensities, which can be can used as proxy for detecting varying dynamics in the case of non-deuterated proteins (Solt et al., 2017). Whereas the increase in molecular weight and the dilution effect upon RNA addition were expected to induce a uniform 13% drop, the M71 (CAT-PRD1 linker), M169 (PRD2) and M179 (PRD2) peak intensities showed decreases higher than 30% (Figure 4E). As these methyl groups are located far away from the interaction site, these decreases illustrate a change in their dynamics and/or structure upon binding to RNA.

By contrast to LicT*, *sym*-RAT binding caused significant changes in native LicT spectrum (Figures 4F). The M25 correlation peak shifted to a position close to the position observed for activated LicT* bound to RNA (although closer inspection revealed the presence of at least two peaks), as did M71 peak. As for RNA-bound LicT*, the M179 correlation peak vanished. Hence, there is a similarity between RNA complexes of LicT and LicT*. However, the RNA complex with inactive LicT apparently exhibits more dynamics than does the complex with LicT*, even for the modules not involved in RNA binding. For example, we noted that the M169 correlation peak (PRD2) almost completely disappeared upon complex formation.

Discussion.

Histidine phosphorylation plays a major role in many cell signaling pathways in prokaryotes and eukaryotes (Kee and Muir, 2012; Makwana et al., 2018). However because of chemical instability, only a few structures of phosphohistidine-containing proteins have been reported (see for example Bond et al., 2001; Jones et al., 2008; van Nuland et al., 1995; Weiße et al., 2016). Accordingly, structural

investigation on the phosphorylation-based regulation of BglG antiterminators has essentially been performed on phosphomimetic mutants, most often on protein fragments. *In vitro* phosphorylation of BglG-like antiterminators has been performed (Lindner et al. 1999, Himmel et al., 2012b; Knezevic et al., 2015; Rothe et al., 2012) but the structural consequences of these phosphorylations have usually not been examined. So far, only NMR studies on the PRD1 module of the GlcT antitermination protein have provided direct structural evidence of histidine phosphorylation for this protein family (Himmel et al., 2012b). In this work, we present the conformational and functional investigation on the activating phosphorylation of full-length LicT. By combining NMR and fluorescence spectroscopy, we demonstrate *in vitro* the link between the phosphorylation of the PRD2 module, the structural reorganization of the full-length protein and its RNA-binding capacities.

Our study pinpoints however structural and functional differences between proteins activated by phosphorylation and by phosphomimetic mutations. This could be due to incomplete phosphorylation under the *in vitro* conditions we used. However, the NMR analysis yielded a phosphorylation rate around 80% and 60% for LicT concentration of 80 and 300 μM, incompatible with this hypothesis. On the other hand, mass spectrometry analysis detected phosphorylation at histidine residues other than those targeted by the *B. subtilis* PTS general components in PRD2. In particular, H100 in PRD1, which is predicted to be the site of negative regulation, could act antagonistically to the activating phosphorylations. However, the mass spectrometry analyses reported in previous quantitative studies (Lindner et al., 1999) suggest that the level of H100 phosphorylation is marginal. In our study, the ^{1}H-^{13}C correlation peaks of M71 and M139 in the PRD1 module of LicT-P correspond to those of LicT*, supporting also a negligible phosphorylation on PRD1 histidines, in accordance with the fact that PRD1 histidines are known to be phosphorylated by EII and not by E1/HPr. Hence, we propose that the spectral differences we observed between the two activation processes rather reflect differences in dynamics at the PRD2 interface, related to differences in antitermination efficacy *in vivo* (Tortosa et al., 2001a) and RNA binding *in vitro* (Figure 3A).

We also present an insight into the architecture of the complex formed by full-length LicT with RNA. RNA binding to LicT* did not produce significant structural changes in the CAT module, demonstrating that the latter is the RNA-binding competent one. For native LicT, RNA binding forces the CAT domain

to switch from its open configuration to a closed dimeric structure (or an ensemble of closed ones). Interestingly, RNA binding provoked changes in the conformation and/or dynamics of the distal PRD2 module for both LicT* and LicT. This allosteric phenomenon may help the de-phosphorylation of the RNA-bound protein, and thus its recycling once transcription is completed.

In addition, fine differences were found between the structures of the effector domain, whether it is isolated or followed by one or two PRD modules. The active structure of CAT in its isolated form was closer to its active form in the bi-modular CAT-PRD1* construct, the latter in turn being closer to its active form in the full-length protein. The "inactive" state of CAT was even less structurally conserved between the bi-and tri-modular proteins, potentially because of a variability of openness. Hence, the regulatory modules exert a fine allosteric effect *per se* on the RNA-binding module.

Altogether, our data establishes the structural mechanism of LicT phosphorylation-driven activation, previously hypothesized from fragment and mutant proteins. It illustrates how structural restraints are back- and forward-propagated between LicT RNA-binding domain and regulatory modules. In this regard, it may help to understand the mechanism of signal transduction for other virulence factors containing PRD-domains such as AtxA of *Bacillus anthracis* (Hammerstrom et al., 2011) or Mga of *Spectrococcus A* (Hondorp et al., 2013), and more generally for modular proteins.

Acknowledgments

The CBS is a member of the French Infrastructure for Integrated Structural Biology (FRISBI), supported by the National Research Agency (ANR-10-INBS-05) and is a GIS-IBIsA platform**.** We thank Serge Urbach and the Functional Proteomics Platform of Institut de Génomique Fonctionnelle (Montpellier) for the mass spectrometry analyses.

Author contributions

Y.Y. and A.P. performed and analyzed NMR experiments. L.M., K.G., N.D. and H.D. purified the proteins. J.G. built the structural models. N.D. performed the phosphorylation and fluorescence anisotropies experiments. N.D. and H.D. designed the experiments and wrote the paper.

Declaration of Interests

The authors declare no competing interest

Figure legends

Figure 1. Modular organization and models of LicT.

(A) Organization of LicT. LicT is composed of an RNA binding domain (CAT) followed by a linker region (black box) and two homologous PTS regulation domains (grey boxes), PRD1 and PRD2. Methionine and phosphorylatable histidines are numbered. For purification needs, an hexa-histidine tag, that is represented here as a squared H and contains one additional terminal methionine called M0, has been added in the N-terminal sequence (Declerck et al., 2001). The structure resolution methods are indicated beneath.

(B) Models of the full length native LicT and of the activated mutant LicT* carrying the H207D/H269D phosphomimetic mutations in PRD2, derived from the individual module structures (Déméné et al., 2008; Graille et al., 2005; van Tilbeurgh et al., 2001; Yang et al., 2002). The model of native LicT presents an open configuration for the CAT dimer, a helical structure for the linker between CAT and PRD1, and a dimeric structure for the PRD1-PRD2 bi-modules with loose inter-dimeric contacts. The model of activated LicT* has a compact and closed dimeric configuration for the CAT and the PRD1-PRD2 modules and a loose CAT-PRD1 linker. Methionine methyl groups are represented as green or orange spheres, for protomers colored in light and dark grey, respectively. Methionine residues with underscored labels belong to the dimerization interface, as estimated from the Protein Interaction Calculation software (Tina et al., 2007). The side chains of the conserved phosphorylatable regulatory histidines (H100 and H159 in PRD1, H207 and H269 in PRD2) are colored in pink and shown in stick representation.

Figure 2. NMR characterization of native LicT and phosphomimetic mutant LicT*

(**A**) Zoom into the methyl region of ^{1}H NMR spectra recorded for CAT, inactive CAT-PRD1, mutant CAT-PRD1*, native LicT and mutant LicT*. V23 methyl group of active CAT and CAT-PRD1* resonate at -0.4 ppm. V23 methyl groups of inactive CAT-PRD1 resonate at 0.8 ppm, outside the spectral range shown here. As insert is pictured a zoom into the closed structure of isolated CAT (Yang et al., 2002), with the side chain of V23 of one protomer (red) and of F48 of the other protomer

(blue) shown as sticks. Protomer backbones are represented as ribbon representation (light and dark grey). The close proximity of these side chains explains the high-field shift of V23 methyl resonances in the closed configuration of CAT. This high field resonance is retrieved in the spectrum of LicT* but not of native LicT.

(B-E) Superposition of the ^{15}N HMQC fingerprints of (**B**) isolated CAT and activated mutant full-length LicT*, (**C**) isolated CAT and native full-length LicT, **(D**) mutant PRD1-PRD2* and mutant LicT*, and (**E**) native PRD1-PRD2 and native LicT. In (**B**) and (**C**), red boxes indicate the position of correlation peaks of the eight residues characteristic of CAT closing. (see also Figure S1 for details).

(**F-G**) Superposition of ^{1}H-^{13}C HMQC spectra of ^{13}C-CH_3-ε-Met labeled (**F**) LicT*, mutant PRD1-PRD2* and isolated CAT, (**G**) native LicT and PRD1-PRD2. The assignment for the full-length proteins is described in Figure S2. Boxed labels refer to peaks which differ the most between LicT and LicT*.

Figure 3. Activation of LicT by PTS-mediated phosphorylation.

(A) Fluorescence anisotropy titrations of Atto647N-labeled *licS*-RAT RNA (0.5 nM, sequence in Figure S4A) by native LicT or the activated mutant LicT* after incubation in the phosphorylation buffer in the absence (dotted lines) or presence (plain lines) of the purified PTS general components EI and HPr. Data were fitted using a simple binding model, or when appropriate, a double binding model of high (nM) and low (μM) affinity as previously described (Ait-Bara et al., 2017).

(B) SEC elution profiles of native LicT and activated LicT* before (LicT and LicT*) and phosphorylation (LicT-P and LicT*-P). Proteins submitted to phosphorylation were separated from the PTS enzymes by SEC before loading on Superdex HR10-300 column for analytical gel filtration. See Figure S3 for an analysis of phosphorylated sites by mass spectrometry.

(C) Zoom into the methyl region of ^{1}H NMR spectra recorded for LicT and LicT* before (LicT and LicT*) and after (LicT-P and LicT*-P) phosphorylation (and subsequent purification).

(D-E) Superposition of ^{1}H-^{13}C HMQC spectra of ^{13}C-CH_3-ε-Met labelled (**D**),LicT-P and LicT*; (**E**), LicT-P and LicT. Blue and black squares refer to the position of the five characteristic correlation peaks of the dimeric configuration (M25, M71, M139, M179 and M221) of phosphomimetic LicT* and native LicT respectively. The experiment was then repeated at higher concentration of LicT (Figure S3).

Figure 4. RNA binding by native LicT and activated mutant LicT*.

(**A**) NMR structure of the complex between isolated CAT and its *licS*-RAT target (Yang et al., 2002) . Each protomer (blue/red) of the CAT homodimer interacts with one of the 2 asymmetric internal loops of the RAT hairpin shown in panel (B). The side-chains of the two methionines (M1 at the N-terminus and M25 at the dimer interface) are shown as yellow and green sticks in each CAT protomer. The two nucleotides that bulge out from the RNA helix in the complex are shown in blue (U8 in loop 1) or pink stick (A26 in loop 2).

(**B**) Sequence of *licS*-RAT and the derived *sym*-RAT used for NMR. *sym*-RAT is predicted to fold as a symmetric hairpin with two identical internal loops corresponding to the conserved *licS*-RAT loop 2. The symmetry of the CAT homodimer is expected to be preserved upon *sym*-RAT binding, preventing doubling of the CAT NMR peaks. The red spheres indicate the position of the Atto647N label introduced for fluorescence anisotropy experiments.

(**C**) Fluorescence anisotropy titrations of Atto647N-labelled *licS*-RAT (open symbols) and *sym*-RAT (plain symbols) by isolated CAT, native LicT and activated mutant LicT*. A simple binding model was used for data fitting except for the LicT*/*licS*-RAT interaction.

(**D-F**) superposition of 2D ^{1}H-^{13}C spectra of mutant apo and *sym*-RAT bound LicT* (**D**), of 1D projections taken across the ^{13}C dimension of Met peaks of LicT* (blue: apo, red: sym-RAT bound) (**E**) and of 2D ^{1}H-^{13}C spectra of native apo and *sym*-RAT bound LicT (**F**). On 2D spectra, blue, pink and black squares refer to the methionine peaks observed for apo LicT*, RNA-bound LicT* and apo LicT, respectively.

Table 1. Dissociation constant of LicT constructs with RNA

	Kd (nM) [a]	
Proteins /RNA	*licS*-RAT	*sym*-RAT
LicT	93 ± 21 [b]	~2000 [f,g]
LicT + (EI,HPr)	6.8 ± 4.3 [c]	ND [h]
LicT*	1.7 ± 0.6 [d]	88 ± 11 [f]
LicT* + (EI,HPr)	1.5 ± 0.8 [e]	ND [h]
LicT-CAT	4.7 ± 0.5 [f]	230 ± 10 [f]

[a] Kd values calculated for the first binding event (highest affinity)
Mean and standard deviation calculated from a total of:
[b] 9 independent experiments using 3 different protein preparations
[c] 7 independent experiments using 2 different protein preparations
[d] 4 independent experiments using 2 different protein preparations
[e] 3 independent experiments using 2 different protein preparations
[f] 2 independent experiments using the same protein preparation
[g] Kd value estimated using the plateau value observed for the LicT*/*sym*-RAT titration curve
[h] Not determined

STAR* METHODS

KEY RESOURCES

REAGENT or RESOURCE	SOURCE	IDENTIFIER
Bacterial and Virus Strains		
BL21(DE3)	Invitrogen TM	CAT# C600003
Chemicals, Peptides, and Recombinant Proteins		
^{13}C-CH_3-ε- labelled methionine	Sigma-Aldrich	CAT# 299146
Lys-C endopeptidase	Wacko	CAT# 129-02541
$^{15}NH_4Cl$	Cambridge Isotope Laboratories	CAT-467-10
^{13}C-glucose	Cambridge Isotope Laboratories	CAT# 110187-4263
Phophosphoenol Pyruvate	Sigma	CAT# 860077
Oligonucleotides		
Atto647N-UGGUAG GAUUGU UACUGA UAAAGC AGGCAA AACCUA AAUCCU CAGACC GCACAC GAUGCG C	Molecular probe	N/A
Atto647N-UGCGGG CUGUUA CCGCUU CGGCGG GCAGUU ACCGC	Molecular Probe	N/A
Recombinant DNA		
pQE30 (full length LicT and LicT*)	Qiagen	N/A
pET15b (CAT, CAT-PRD1, CAT-PRD1*, E1, HPr)	Novagen	Cat# 69661
Software and Algorithms		
Gifa	Pons et al. 1996	http://abcis.cbs.cnrs.fr/DOWNLOAD/Gifa5/
Nmrview	Johnson and Blevins, 1994	http://samtools.sourceforge.net
PIC	(Tina et al., 2007)	http://pic.mbu.iisc.ernet.in/
RosettaRemodel	Huang et al. 2011	http://www.rosettacommons.org/.

Other		
PRD1-PRD2 structure (native)	Protein Data Bank (PDB)	PDB code 1TLV
PRD1-PRD2 structure (activated)	PDB	PDB code 1H99
CAT structure	PDB	PDB code 1L1C
Model of Full length activated LicT-H207D/H269D *	This study	Available on request
Model of Full length of native LicT*	This study	Available on request

LEAD CONTACT AND MATERIALS AVAILABILITY

Further information and requests for resources and reagents should be directed to and will be fulfilled without restriction by the Lead Contact, Helene Déméné (Helene.demene@cbs.cnrs.fr)

EXPERIMENTAL MODEL AND SUBJECT DETAILS.

Bacterial Strains

All LicT constructs and the E1 and HPr enzymes were expressed in commercially purchased Escherichia coli BL21(DE3).

METHOD DETAILS

Protein purification

All LicT and PTS proteins were expressed as histidine-tagged proteins in *E. coli* BL21(DE3). They were purified using HisTrap HP columns (GE Healthcare, Piscataway, NJ) and gel filtration on a Superdex 75 column (GE Healthcare, Piscataway, NJ) as previously described (Declerck et al., 2001; Ducat et al., 2002; Tortosa et al., 2001b). ^{15}N- labelled proteins were obtained by growing cells in M9 minimal media with ^{15}N ammonium chloride (Eurisotop, St Aubin, France) as the unique source of nitrogen. and ^{13}C glucose (Eurisotop, St Aubin, France) was also added as the sole source of carbonated substrate for production of ^{15}N, ^{13}C fully labelled samples. ^{13}C-labelled Methyl-protonated samples on methionines

were prepared by adding $^{1}H,^{13}C$ Methionine-ε-CH_3 (Sigma) at 250 mg/L, 30 min to the M9 medium prior the induction period of 2 hours (Tzeng et al., 2012).

NMR spectroscopy

All NMR experiments were performed at 305 (^{15}N-labelled) and 293 K (^{13}C-Met-labelled) on a Bruker 700 MHz Avance III spectrometer (Bruker, Rheinstetten, Germany) using a 5 mm triple resonance cryogenic probe with Z-axis gradient. Proton chemical shifts were referenced with respect to DSS (Sigma) and the frequency ratios of $^{15}N/^{1}H = 0.101329118$ and $^{13}C/^{1}H = 0.251449530$. ^{15}N HMQC experiments were typically recorded at a 200 μM concentration, whereas the concentration of ^{13}C-^{1}H HMQC spectra ranged from 50 μM for the RNA titration to 300 μM (phosphorylation). NMR spectra were processed using the Gifa program (Pons et al., 1996) and analyzed using NMRView (Johnson and Blevins, 1994). 1D (^{15}N-^{1}H) TRACT experiments on ^{15}N-LicT* (Lee et al., 2006) were recorded with an interscan delay of 3s, 512 transients and relaxation delays ranging from 3 to 48 ms. The relaxation rates Rα and Rβ were obtained by fitting a single exponential to the integrals over the backbone amide proton region starting from 9 ppm to 8 ppm.

Modeling

Structural models of full-length LicT were constructed using as templates the crystal structure of the RNA-binding domain CAT (to be published) and the crystal structures of the regulatory modules (PRD1-PRD2) in the native state (PDB code 1TLV) or activated mutant state (PDB code 1H99). The linker between the CAT and PRD1 protomers was built using the REMODEL program from the Rosetta modeling suite (Huang et al., 2011). For the native state, the central linker residues 55-61 were constrained in helix states while their flanking residues 51-54 and 62-65 were assigned to loop states, according to the chemical shift-derived structural propensity. The first chain of the dimer built by REMODEL was then duplicated to build a symmetrical complex according to the C2 symmetry axis of the X-Ray structure. Finally, the CAT-PRD1 linker sidechain conformations of the symmetrical dimer were further optimized by energy minimization using the Remodel rotamer sampling level "EX 2" (Huang et al., 2011).

The active conformation of the CAT-PRD1 linker was modeled for different orientations and of the CAT dimer (1G03) relatively to active form of the PRD1-PRD2 dimer (1H99). To this end, the symmetry axis and the symmetry plane of both dimers were superposed and different values of the distance and rotation angle between both dimers were tested. For each possible arrangement, the two linkers connecting CAT to PRD1 were modeled as done for the inactive model, except for the fact that the linker residues were constrained to loop states, as inferred from our previous structural studies of CAT-PRD1 modules (Déméné et al., 2008).

Phosphorylation assays

Phosphorylation reactions were performed in 50 mM Tris buffer pH 7.5 in the presence of 200 mM NaCl, 10 mM $MgCl_2$ and 5 mM PEP (Sigma). The purified LicT proteins were typically added at a final concentration of 40 µM, and the purified PTS enzyme I (EI) and phosphocarrier proteins (HPr) from *B. subtilis* at a final concentration of 6 and 20 µM, respectively. Samples were incubated for 2 h at 37°C then left overnight at room temperature. The phosphorylation reactions were eventually concentrated and loaded on a Superdex 75 10-300 GL (GE Healthcare) in order to eliminate the PTS enzymes. For the NMR characterization, two concentrations of LicT of 80 and 300 µM were used, at LicT/EI/HPr ratios of 4/0.6/2 and of 4/0.2/0.5 respectively.

SEC-MALS analysis

The oligomerization state of proteins was analyzed using an AKTA HPLC-MALS apparatus. 50 µl proteins samples at 4 mg/ml were loaded onto a Superdex 75 10/300 gel-filtration column (GE-Healthcare) equilibrated at 0.5 ml/min with the NMR buffer. The eluate was passed successively through a UV 900 GE monitor, a Wyatt Optilab rEX refractive index monitor and a Wyatt miniDawn TREOS 3-angle light-scattering Data were processed and molecular masses calculated with the Astra 6.1 software (Wyatt).

RNA binding assays.

The RNA binding activity of the LicT proteins was monitored by fluorescence anisotropy as previously described (Clerte et al., 2013). Fluorescence anisotropy titrations were performed in Corning NBS 384-

well plates by adding 40 µL of the Atto647N-labelled synthetic RNA probe (Molecular Probe) to 40 µL of protein serial dilutions in 20 mM Tris pH 8, 200 mM NaCl, 1 mM DTT and 0.1 mg/mL Bovine Serum Albumin. Fluorescence polarization was measured at 25°C using a Tecan Saphire II microplate reader, with the excitation set at 630 nM and the emission at 680 nm +/- 10 nm. Affinity constants were estimated by fitting the titration curves using either a two-site or one-site affinity model (Ait-Bara et al., 2017).

Mass spectrometry

For each sample, 5 µg of protein were digested overnight at 30°C using Lys-C (Wako). After purification using OMIX C18 (Waters), peptides were analyzed online by nano-flow HPLC-nanoelectrospray ionisation using a Qexactive Plus mass spectrometer (Thermo Fisher Scientific) coupled to a nano- LC system (U3000-RSLC, Thermo Fisher Scientific). Desalting and preconcentration of samples were performed online on a Pepmap® precolumn (0.3 × 10 mm; Dionex). A gradient consisting of 0–40% B in A for 90 min (A: 0.1% formic acid, 2% acetonitrile in water, and B: 0.1% formic acid in acetonitrile) at 300 nl/min was used to elute peptides from the capillary reverse-phase column (0.075 × 150 mm, Pepmap®, Dionex). Data were acquired using the Xcalibur software (version 4.0). A cycle of one full-scan mass spectrum (375–1500 m/z) at a resolution of 70,000 (at 200 m/z), followed by 12 data-dependent MS/MS spectra (at a resolution of 17,500, isolation window 1.2 m/z) was repeated continuously throughout the nanoLC separation. Raw data analysis was performed using the MaxQuant software (version 1.5.5.1) with standard settings and phospho-histidine added as variable modification (neutral loss -98 Da). Used database consists of *E. coli* entries from Uniprot**,** Lict and LicT* sequences and 250 contaminants (MaxQuant contaminant database).

QUANTIFICATION AND STATISTICAL ANALYSIS

Table 1: Kd values were reported as means ± standard deviations from independent experiments (N_{exp}) and different protein preparation (N_{prep}) as reported in the table notes.

LicT/*licS*-RAT, N_{exp} = 9, N_{prot}=3; LicT/*sym*-RAT, N_{exp} = 2, N_{prot}=1; LicT-P/*licS*-RAT, N_{exp} = 7, N_{prot}=2;

LicT*/*licS*-RAT, N_{exp} = 4, N_{prot}=2; LicT*/*sym*-RAT, N_{exp} = 2, N_{prot}=1; LicT*-P/*licS*-RAT, N_{exp} = 3, N_{prot}=2; CAT/*licS*-RAT, N_{exp} = 1, N_{prot}=1; CAT/*sym*-RAT, N_{exp} = 2, N_{prot}=1.

Figure S1: the reproducibility of the comparison of CAT configuration between LicT constructs was assessed by the recording of NMR experiments on 2 different protein preparations (culture and purification, with new freshly prepared buffer solutions). Error in chemical shifts were taken as the standard errors between the two sets of measurements.

DATA AND CODE AVAILABILITY

MS/MS and NMR spectra are available as Supplemental data. This work did not generate any software.

References

Ait-Bara, S., Clerté, C., Declerck, N., and Margeat, E. (2017). Competitive folding of RNA structures at a termination–antitermination site. RNA *23*, 721–734.

Amster-Choder, O., and Wright, A. (1992). Modulation of the dimerization of a transcriptional antiterminator protein by phosphorylation. Science *257*, 1395–1398.

Bahr, T., Luttmann, D., Marz, W., Rak, B., and Gorke, B. (2011). Insight into Bacterial Phosphotransferase System-Mediated Signaling by Interspecies Transplantation of a Transcriptional Regulator. J. Bacteriol. *193*, 2013–2026.

Bond, C.S., White, M.F., and Hunter, W.N. (2001). High Resolution Structure of the Phosphohistidine-activated Form of *Escherichia coli* Cofactor-dependent Phosphoglycerate Mutase. J. Biol. Chem. *276*, 3247–3253.

Clerte, C., Declerck, N., and Margeat, E. (2013). Competitive folding of anti-terminator/terminator hairpins monitored by single molecule FRET. Nucleic Acids Res. *41*, 2632–2643.

Declerck, N., Dutartre, H., Receveur, V., Dubois, V., Royer, C., Aymerich, S., and Van Tilbeurgh, H. (2001). Dimer stabilization upon activation of the transcriptional antiterminator LicT. J. Mol. Biol. *314*, 671–681.

Déméné, H., Ducat, T., De Guillen, K., Birck, C., Aymerich, S., Kochoyan, M., and Declerck, N. (2008). Structural mechanism of signal transduction between the RNA-binding domain and the phosphotransferase system regulation domain of the LicT antiterminator. J. Biol. Chem. *283*, 30838–30849.

Deutscher, J., Francke, C., and Postma, P.W. (2006). How Phosphotransferase System-Related Protein Phosphorylation Regulates Carbohydrate Metabolism in Bacteria. Microbiol. Mol. Biol. Rev. *70*, 939–1031.

Ducat, T., Declerck, N., Kochoyan, M., and Déméné, H. (2002). 1H, 15N and 13C backbone resonance assignments of the 40 kDa LicT-CAT-PRD1 protein. J. Biomol. NMR *23*, 325–326.

Galinier, A., and Deutscher, J. (2017). Sophisticated Regulation of Transcriptional Factors by the Bacterial Phosphoenolpyruvate: Sugar Phosphotransferase System. J. Mol. Biol. *429*, 773–789.

Görke, B., and Stülke, J. (2008). Carbon catabolite repression in bacteria: Many ways to make the most out of nutrients. Nat. Rev. Microbiol. *6*, 613–624.

Graille, M., Zhou, C.-Z., Receveur-Bréchot, V., Collinet, B., Declerck, N., and van Tilbeurgh, H. (2005). Activation of the LicT Transcriptional Antiterminator Involves a Domain Swing/Lock Mechanism Provoking Massive Structural Changes. J. Biol. Chem. *280*, 14780–14789.

Hammerstrom, T.G., Roh, J.H., Nikonowicz, E.P., and Koehler, T.M. (2011). Bacillus anthracis virulence regulator AtxA: oligomeric state, function and CO2-signalling. Mol. Microbiol. *82*, 634–647.

Himmel, S., Grosse, C., Wolff, S., Schwiegk, C., and Becker, S. (2012a). Structure of the

RBD-PRDI fragment of the antiterminator protein GlcT. Acta Crystallogr. Sect. F Struct. Biol. Cryst. Commun. *68*, 751–756.

Himmel, S., Zschiedrich, S., Becker, S., Hsiao, H.-H., Wolff, C., Diethmaier, C., Urlaub, H., Lee, D., P.Griesinger, C., and Stülke, J. (2012b). Determinants of Interaction Specificity of the Bacillus subtilis GlcT Antitermination Protein. J. Biol. Chem. *287*, 27731–27742.

Hondorp, E.R., Hou, S.C., Hause, L.L., Gera, K., Lee, C.-E., and McIver, K.S. (2013). PTS phosphorylation of Mga modulates regulon expression and virulence in the group A streptococcus. Mol. Microbiol. *88*, 1176–1193.

Huang, P.-S., Ban, Y.-E.A., Richter, F., Andre, I., Vernon, R., Schief, W.R., and Baker, D. (2011). RosettaRemodel: A Generalized Framework for Flexible Backbone Protein Design. PLoS One *6*, e24109.

Johnson, B.A., and Blevins, R.A. (1994). NMR View: A computer program for the visualization and analysis of NMR data. J. Biomol. NMR *4*, 603–614.

Jones, B.E., Rajagopal, P., and Klevit, R.E. (2008). Phosphorylation on histidine is accompanied by localized structural changes in the phosphocarrier protein, HPr from Bacillus subtilis. Protein Sci. *6*, 2107–2119.

Kee, J.-M., and Muir, T.W. (2012). Chasing phosphohistidine, an elusive sibling in the phosphoamino acid family. ACS Chem. Biol. *7*, 44–51.

Knezevic, I., Bachem, S., Sickmann, A., Meyer, H.E., Stülke, J., and Hengstenberg, W. (2015). Regulation of the glucose-specific phosphotransferase system (PTS) of Staphylococcus carnosus by the antiterminator protein GlcT. Microbiology *146*, 2333–2342.

Lee, D., Hilty, C., Wider, G., and Wüthrich, K. (2006). Effective rotational correlation times of proteins from NMR relaxation interference. J. Magn. Reson. *178*, 72–76.

Lindner, C., Galinier, A., Hecker, M., and Deutscher, J. (1999). Regulation of the activity of the Bacillus subtilis antiterminator LicT by multiple PEP-dependent, enzyme I- and HPr-catalysed phosphorylation. Mol. Microbiol. *31*, 995–1006.

Makwana, M. V, Muimo, R., and Jackson, R.F. (2018). Advances in development of new tools for the study of phosphohistidine. Lab. Invest. *98*, 291–303.

van Nuland, N.A.J., Boelens, R., Scheek, R.M., and Robillard, G.T. (1995). High-resolution Structure of the Phosphorylated Form of the Histidine-containing Phosphocarrier Protein HPr fromEscherichia coliDetermined by Restrained Molecular Dynamics from NMR-NOE Data. J. Mol. Biol. *246*, 180–193.

Pons, J.-L., Malliavin, T., and Delsuc, M. (1996). Gifa V. 4: A complete package for NMR data set processing. J. Biomol. NMR *8*.

Postma, P.W., Lengeler, J.W., and Jacobson, G.R. (1993). Phosphoenolpyruvate:carbohydrate phosphotransferase systems of bacteria. Microbiol. Rev. *57*, 543–594.

Rothe, F.M., Bahr, T., Stulke, J., and Rak, B.Gorke, B. (2012). Activation of Escherichia coli antiterminator BglG requires its phosphorylation. Proc. Natl. Acad. Sci. *109*, 15906–15911.

Rutberg, B. (1997). Antitermination of transcription of catabolic operons. Mol. Microbiol. *23*, 413–421.

Solt, A.S., Bostock, M.J., Shrestha, B., Kumar, P., Warne, T., Tate, C.G., and Nietlispach, D. (2017). Insight into partial agonism by observing multiple equilibria for ligand-bound and Gs-

mimetic nanobody-bound β1-adrenergic receptor. Nat. Commun. *8*, 1795.

Stülke, J., Arnaud, M., Rapoport, G., and Martin-Verstraete, I. (1998). PRD--a protein domain involved in PTS-dependent induction and carbon catabolite repression of catabolic operons in bacteria. Mol. Microbiol. *28*, 865–874.

van Tilbeurgh, H., Le Coq, D., and Declerck, N. (2001). Crystal structure of an activated form of the PTS regulation domain from the LicT transcriptional antiterminator. EMBO J. *20*, 3789–3799.

Tina, K.G., Bhadra, R., and Srinivasan, N. (2007). PIC: Protein Interactions Calculator. Nucleic Acids Res. *35*, W473-6.

Tortosa, P., Declerck, N., Dutartre, H., Lindner, C., Deutscher, J., and Coq, D. Le (2001a). Sites of positive and negative regulation in the Bacillus subtilis antiterminators LicT and SacY. Mol. Microbiol. *41*, 1381–1393.

Tortosa, P., Declerck, N., Dutartre, H., Lindner, C., Deutscher, J., and Le Coq, D. (2001b). Sites of positive and negative regulation in the Bacillus subtilis antiterminators LicT and SacY. Mol. Microbiol. *41*, 1381–1393.

Tzeng, S.-R., Pai, M.-T., and Kalodimos, C.G. (2012). NMR Studies of Large Protein Systems. In Methods in Molecular Biology (Clifton, N.J.), pp. 133–140.

Weiße, R.H.-J., Faust, A., Schmidt, M., Schönheit, P., and Scheidig, A.J. (2016). Structure of NDP-forming Acetyl-CoA synthetase ACD1 reveals a large rearrangement for phosphoryl transfer. Proc. Natl. Acad. Sci. U. S. A. *113*, E519-28.

Yang, Y., Declerck, N., Manival, X., Aymerich, S., and Kochoyan, M. (2002). Solution structure of the LicT-RNA antitermination complex: CAT clamping RAT. EMBO J. *21*, 1987–1997.

+26

Figure

Figure 1

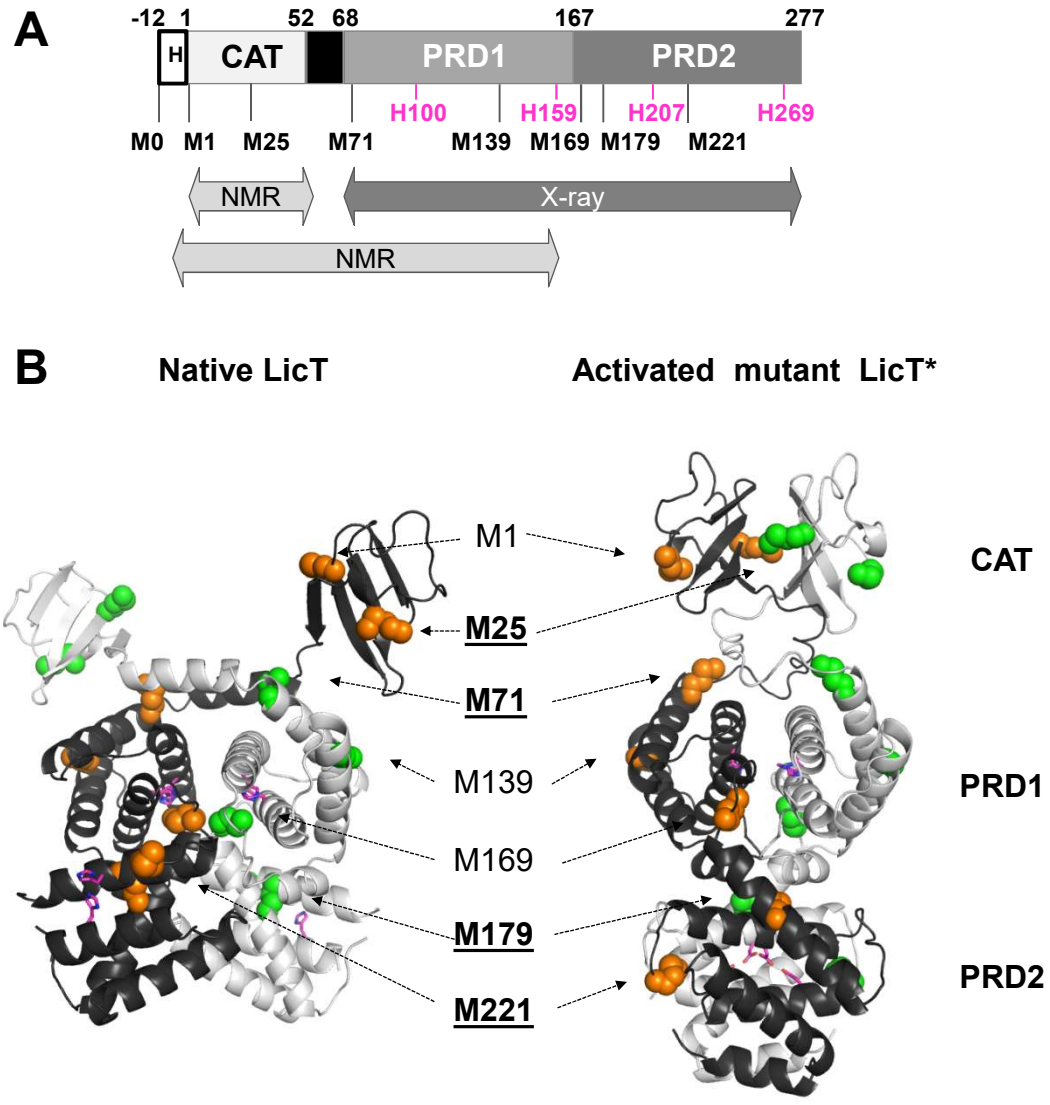

Figure 2

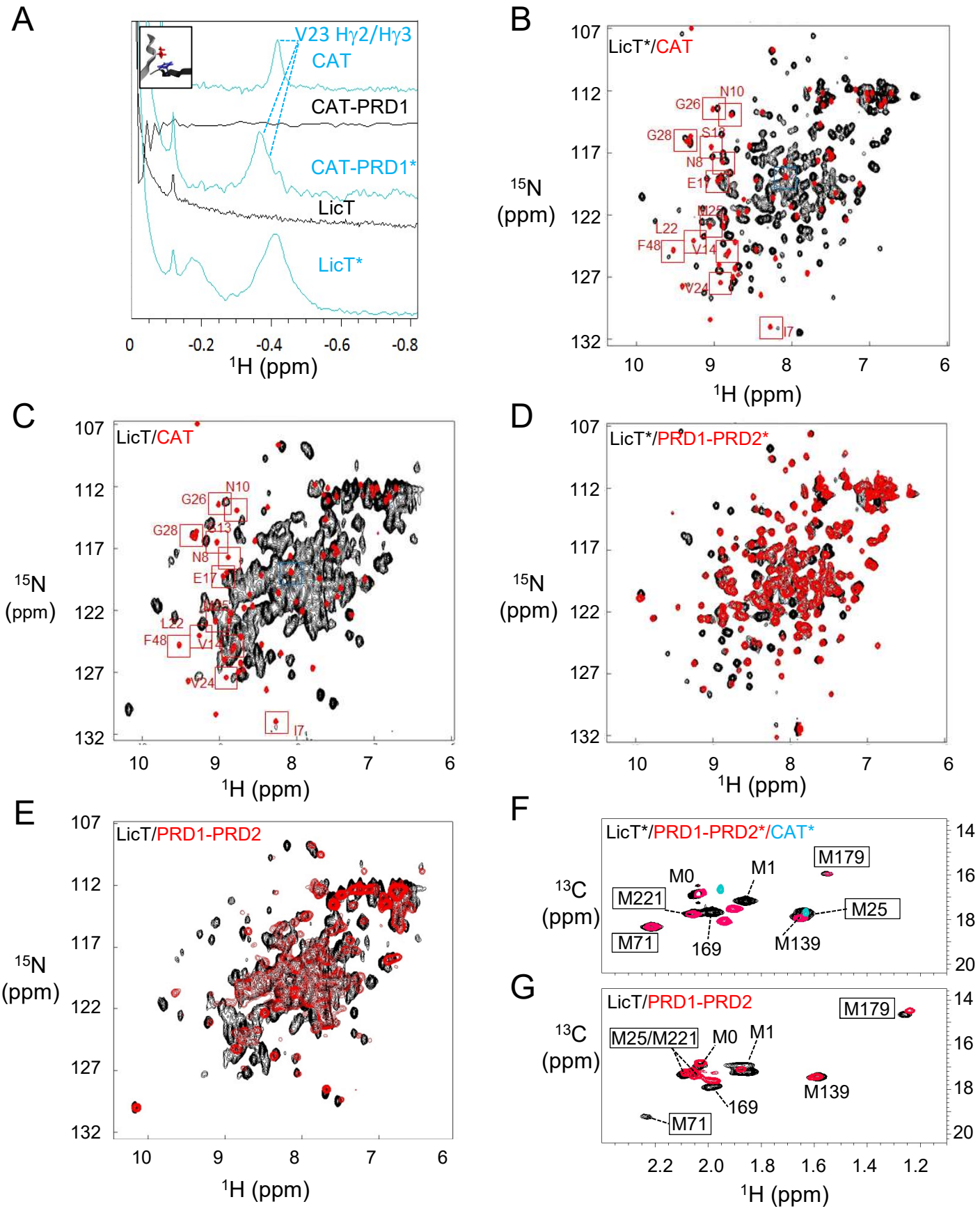
A
V23 Hγ2/Hγ3
CAT
CAT-PRD1
CAT-PRD1*
LicT
LicT*
0
-0.2
-0.4
-0.6
-0.8
1H (ppm)
B
LicT*/CAT
15N (ppm)
107
112
117
122
127
132
10
9
8
7
6
1H (ppm)
N10
G26
G28
S13
N8
E17
M25
L22
F48
V14
V24
I7
C
LicT/CAT
D
LicT*/PRD1-PRD2*
E
LicT/PRD1-PRD2
F
LicT*/PRD1-PRD2*/CAT*
13C (ppm)
14
16
18
20
M179
M0
M1
M221
M25
M71
169
M139
G
LicT/PRD1-PRD2
M25/M221
2.2
2.0
1.8
1.6
1.4
1.2

Figure 3

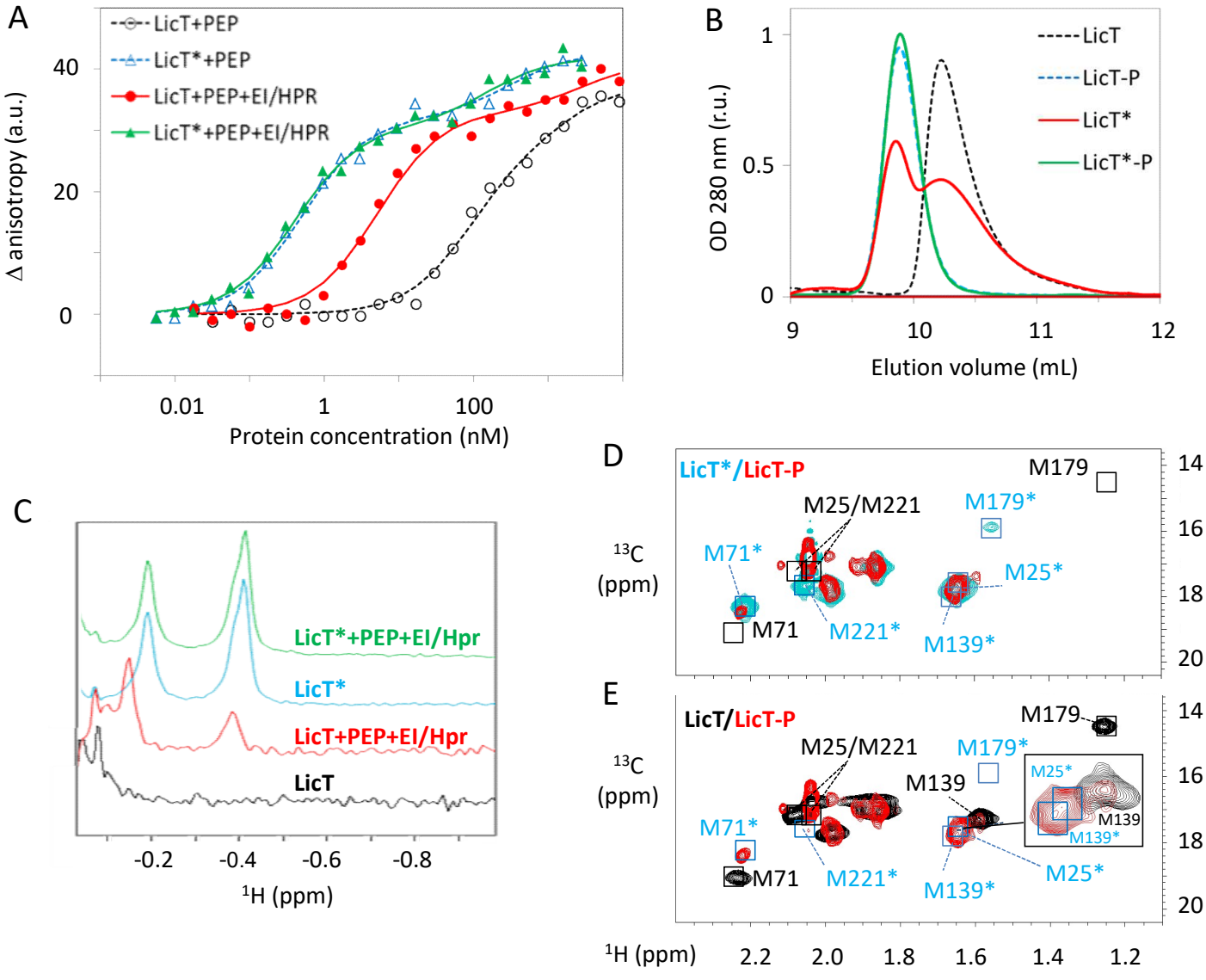
A
LicT+PEP
LicT*+PEP
LicT+PEP+EI/HPR
LicT*+PEP+EI/HPR
Δ anisotropy (a.u.)
40
20
0
0.01
1
100
Protein concentration (nM)
B
LicT
LicT-P
LicT*
LicT*-P
OD 280 nm (r.u.)
1
0.5
0
9
10
11
12
Elution volume (mL)
C
LicT*+PEP+EI/Hpr
LicT*
LicT+PEP+EI/Hpr
LicT
-0.2
-0.4
-0.6
-0.8
¹H (ppm)
D
LicT*/LicT-P
M179
M25/M221
M179*
M71*
M25*
M71
M221*
M139*
¹³C (ppm)
14
16
18
20
E
LicT/LicT-P
M179
M25/M221
M179*
M139
M25*
M139
M139*
M71*
M71
M221*
M139*
M25*
¹³C (ppm)
14
16
18
20
¹H (ppm)
2.2
2.0
1.8
1.6
1.4
1.2

Figure 4

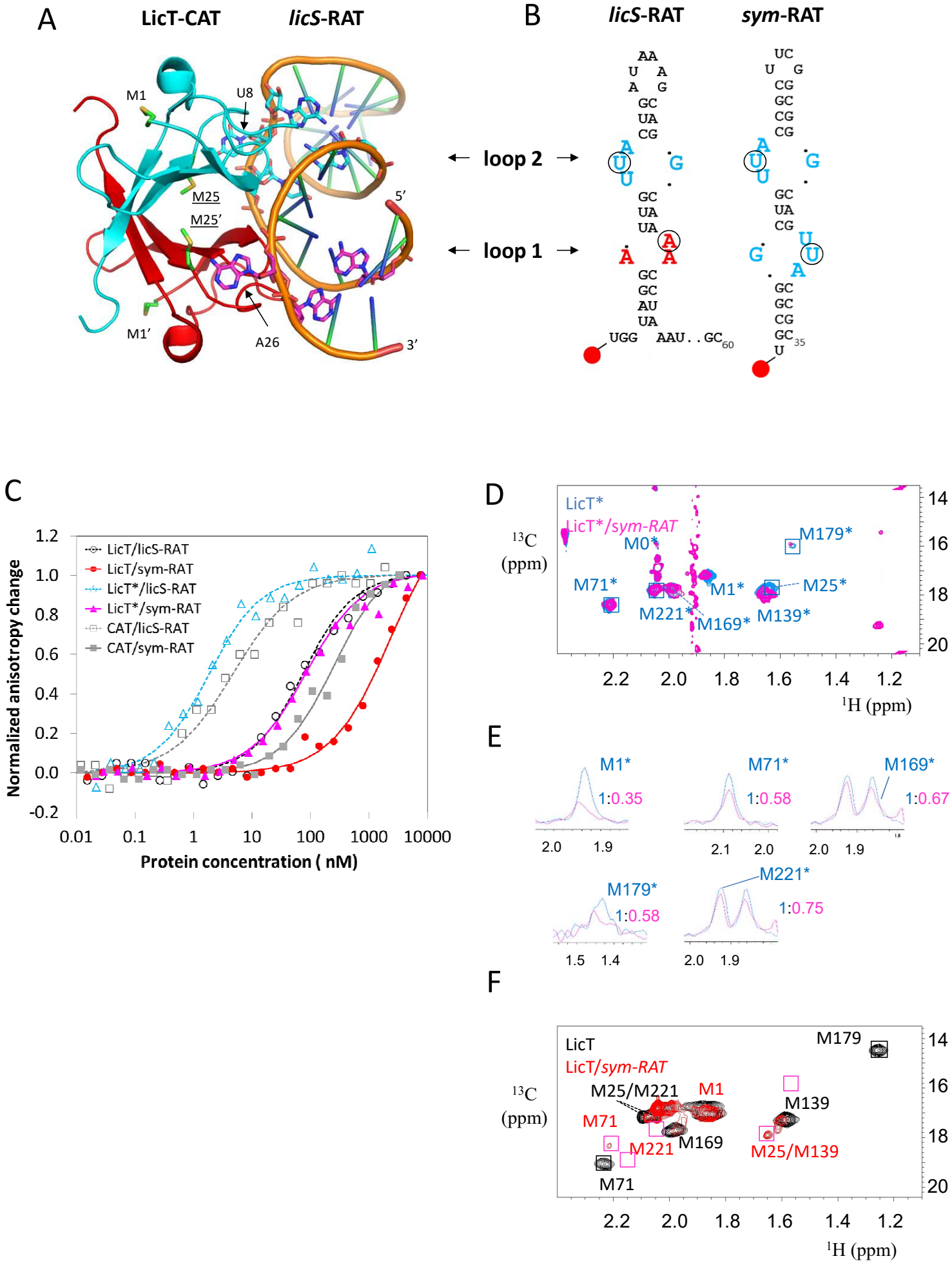
A
LicT-CAT
licS-RAT
M1
U8
M25
M25'
5'
M1'
A26
3'
B
licS-RAT
sym-RAT
loop 2
loop 1
UGG AAU . . GC60
C
Normalized anisotropy change
LicT/licS-RAT
LicT/sym-RAT
LicT*/licS-RAT
LicT*/sym-RAT
CAT/licS-RAT
CAT/sym-RAT
Protein concentration (nM)
D
LicT*
LicT*/sym-RAT
M0*
M179*
M71*
M1*
M25*
M221*
M169*
M139*
13C (ppm)
1H (ppm)
E
M1*
1:0.35
M71*
1:0.58
M169*
1:0.67
M179*
1:0.58
M221*
1:0.75
F
LicT
LicT/sym-RAT
M179
M25/M221
M1
M139
M71
M169
M221
M25/M139
M71
13C (ppm)
1H (ppm)

Figure S1, related to Figure 2.

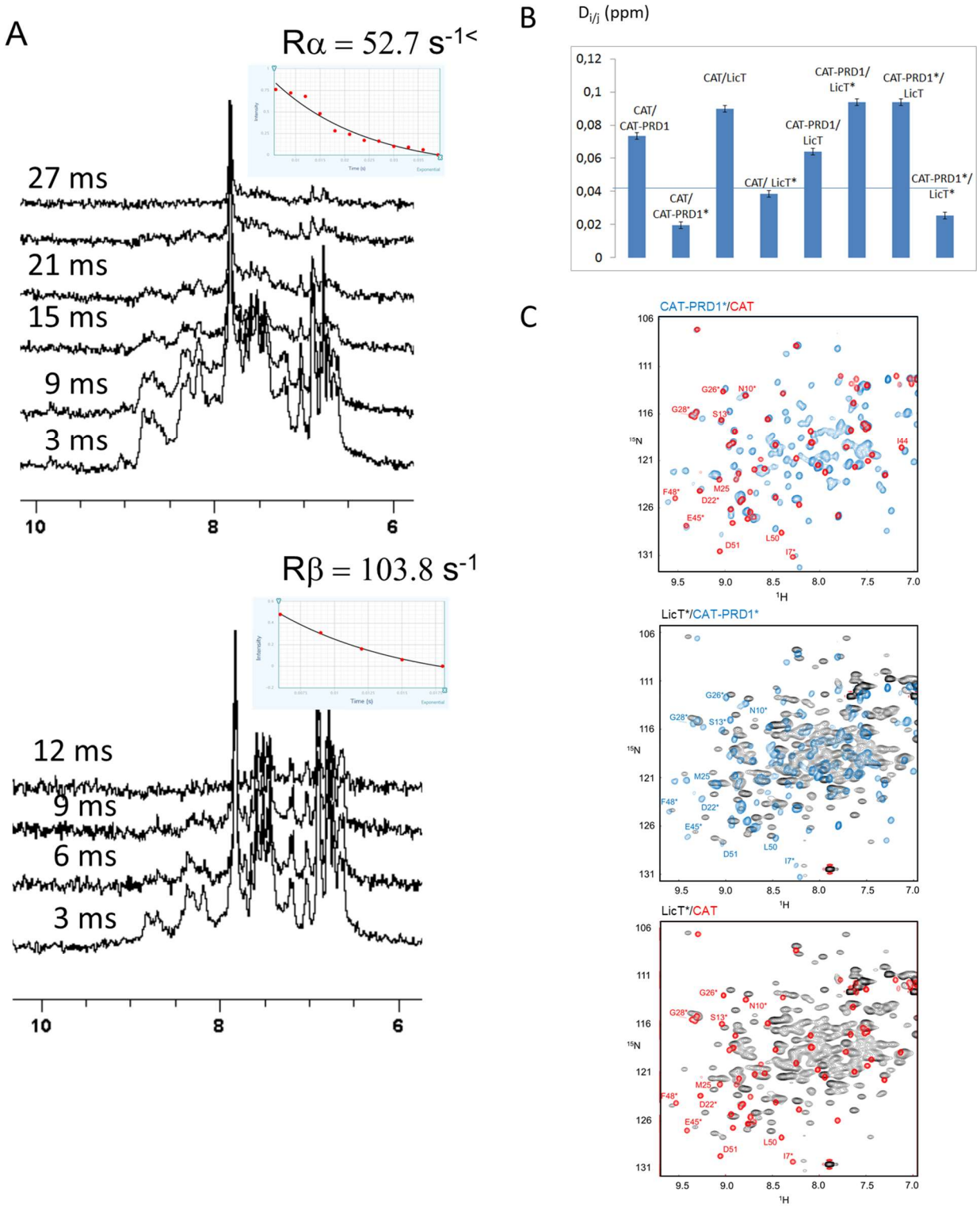

Figure S1. Relaxation analysis of mutant activated LicT* and CAT configuration (related to Figure 2).

(A) Plots of amide regions of 1D TRACT experiments (Lee et al., 2006) of α and β spin states recorded on mutant activated LicT* at 700 MHz for various relaxation periods (indicated on the spectra) at 305 K. The corresponding exponential fittings with the estimated relaxation rates Rα and Rβ are reported as inserted insets. The difference of 51.1 s^{-1} between Rβ and Rα corresponds to a 21.2 ns correlation time and a molecular weight in the 67.5-82.4 kDa range, in accordance with a molecular weight estimated between 64.6 kDa (His-Tag excluded) and 76.2 kDa (His-tag included).

(B) Quantitative measure of the structural discrepancy Di/j between two LicT constructs i and j as the pondered cumulative sum of the pondered chemical shift δ differences averaged for residues I7, N8, N10, S13, E22, G26, G28 and F48 belonging to the dimerization interface of the CAT module.

(C) Comparison of the correlation peaks corresponding to CAT resonances in the superposition of the ^{15}N HMQC fingerprints of isolated CAT and active CAT-PRD1* (above), active CAT-PRD1* and active LicT* (middle) and isolated CAT and active LicT*. Peaks corresponding to the dimeric interface are annotated and annotations labelled with an asterisk * refer to peaks whose resonances were integrated in Di/j calculation (Of note, peaks that could be unambiguously identified on LicT* spectrum were not taken into account to calculate Di/j). The different superimpositions illustrate that the closed CAT configuration is well conserved between the isolated CAT domain and the active CAT-PRD1* protein, less conserved between the active CAT-PRD1* and full length LicT* proteins and even less conserved between the isolated CAT domain and the active full length LicT* protein. This dissimilarity, which seems to be dependent on the number of regulatory modules, points to the structural restraints exerted by the PRD regulatory modules on the CAT effector module.

Figure S2, related to Figure 2

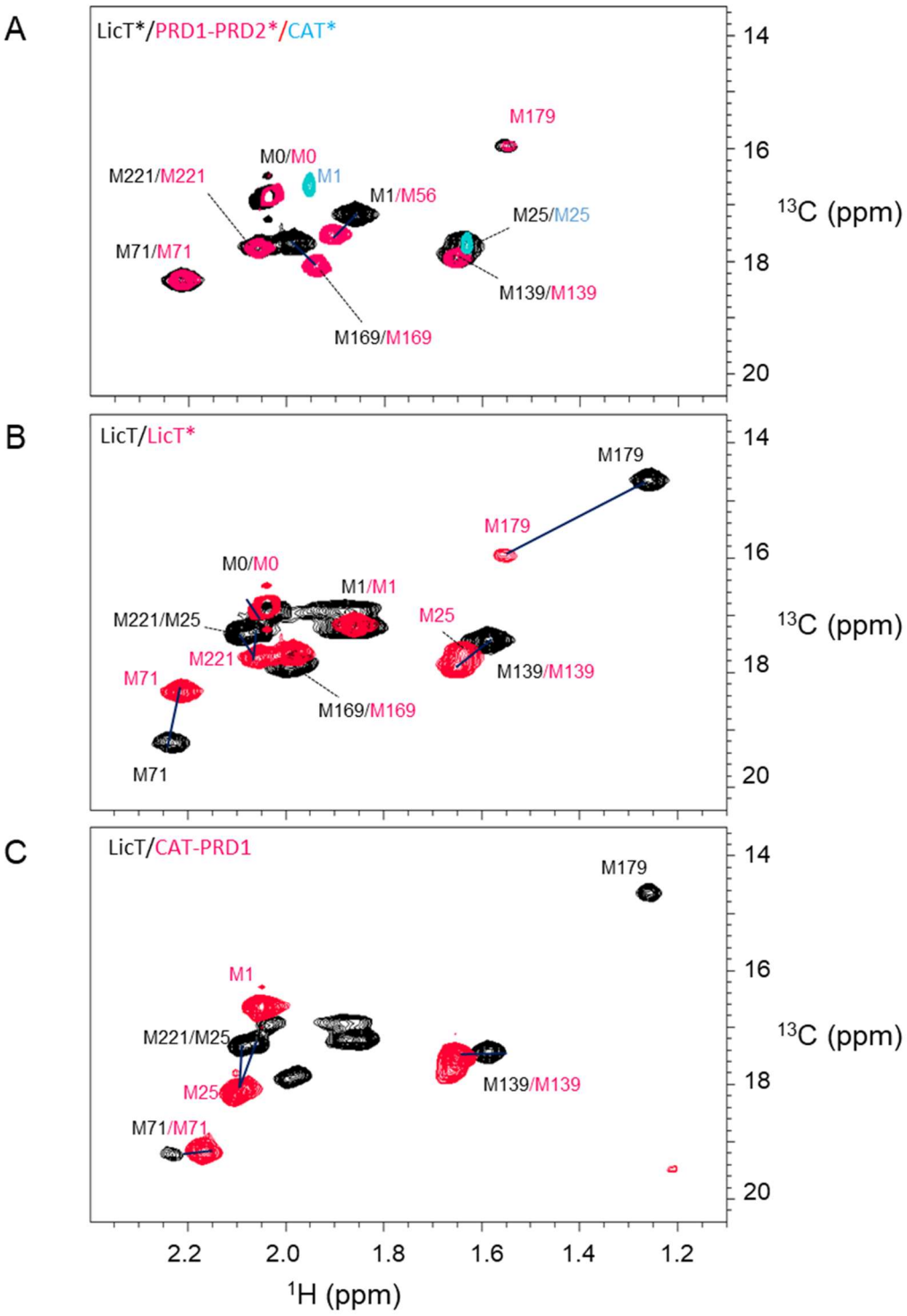

Figure S2. Assignment of $^{13}CH_3$-labelled methionine peaks in different LicT constructs (related to Figure 2).

(A) Methionine peaks of PRD1-PRD2* (red) and of CAT (blue) were assigned using classical triple resonance experiments. Extension to peaks of full-length LicT* (black) was straightforward and is visualized as dark blue plain lines connecting peaks. M56 of PRD1-PRD2* corresponds to an extra methionine residue at the C-extremity of the N-terminal His Tag (**M_0RGSHHHHHHGSM$_{56}$**E), and presents a similar magnetic environment as M1 of LicT*, also located at the C-extremity of the N-terminal His-Tag (**M_0RGSHHHHHHGSM$_1$**K).

(B) M0, M1, M139, M169, M179 and M221 methionine peaks of native LicT could be assigned from the comparison of LicT* (red) and LicT (black) ^{1}H-^{13}C correlation spectra. For M221, there are two candidate correlation peaks which lie side by side.

(C) Methionine peaks of CAT-PRD1 (red) were assigned using classical triple resonance experiments. M139 peak assignment of full-length LicT (panel B) was confirmed. M25 was identified as one of the two candidate peaks for M221.

Figure S3, related to Figure 3

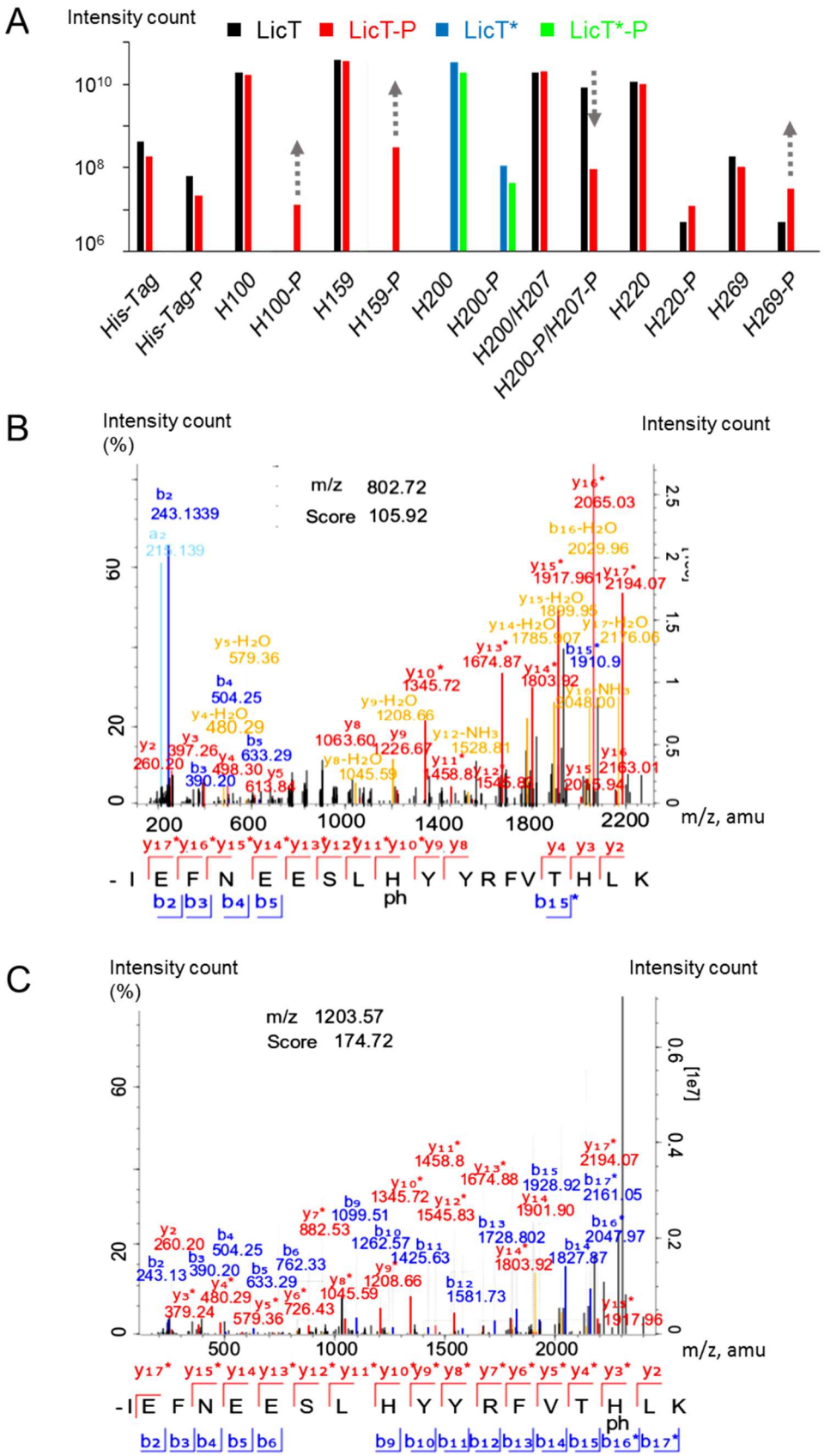

Figure S3. Characterization of LicT phosphorylation by mass spectrometry (related to Figure 3).

(A) Intensity counts of phosphohistidine-containing peptides and their non-phosphorylated counterparts detected by MS/MS spectrometry of LicT and LicT* (carrying the H207D/H269D activating mutation) before and after *in vitro* PEP/EI/HPr-dependent phosphorylation. The up and down arrows indicate phosphorylated peptides whose intensity increases or decreases more than 5 fold after the phosphorylation reaction. Note that for different peptides, relative intensities are not directly related to relative abundances. Compared to their non-phosphorylated counterparts and because of their negative charges, phosphorylated peptides are poorly detected by the nanoelectrospray ionization method used here. Phosphohistidines detected prior to the phosphorylation reaction (H200, H207, H220, H269 and the histidines of the purification tag in LicT, H200 in LicT*) most likely result from endogenous PTS-catalyzed phosphorylation in *E. coli* in which the recombinant proteins were produced. For these particular phosphohistidines, comparison of the phosphorylation levels before and after incubation with the Bacillus subtilis enzymes enables an estimation of the assay efficacy. For the native LicT peptide carrying both H200 and H207, a high level of the mono-phosphorylated forms (with phosphohistidine at either H200 or H207, see panels B and C) was detected prior the phosphorylation reaction. After incubation with the *B. subtilis* PTS enzymes this level dropped by two orders of magnitude while no doubly-phosphorylated peptide was detected. Given the fact that H207 was previously shown to be the major site of LicT PTS-dependent phosphorylation (Lindner et al. 1999), we interpret these data as an evidence for massive phosphorylation of this peptide at position H207, resulting in doubly-phosphorylated peptides that cannot be detected by MS/MS spectrometry due to very low ionization efficiency.

(**B-C**) Annotated MS/MS spectra for phosphorylated peptides of LicT-P identified as IEFNEESLH_{200}YYRFVTH_{207}LK with a phosphohistidine (ph) at position H200 (**B**) or H207 (**C**).

Figure S4, related to Figure 3.

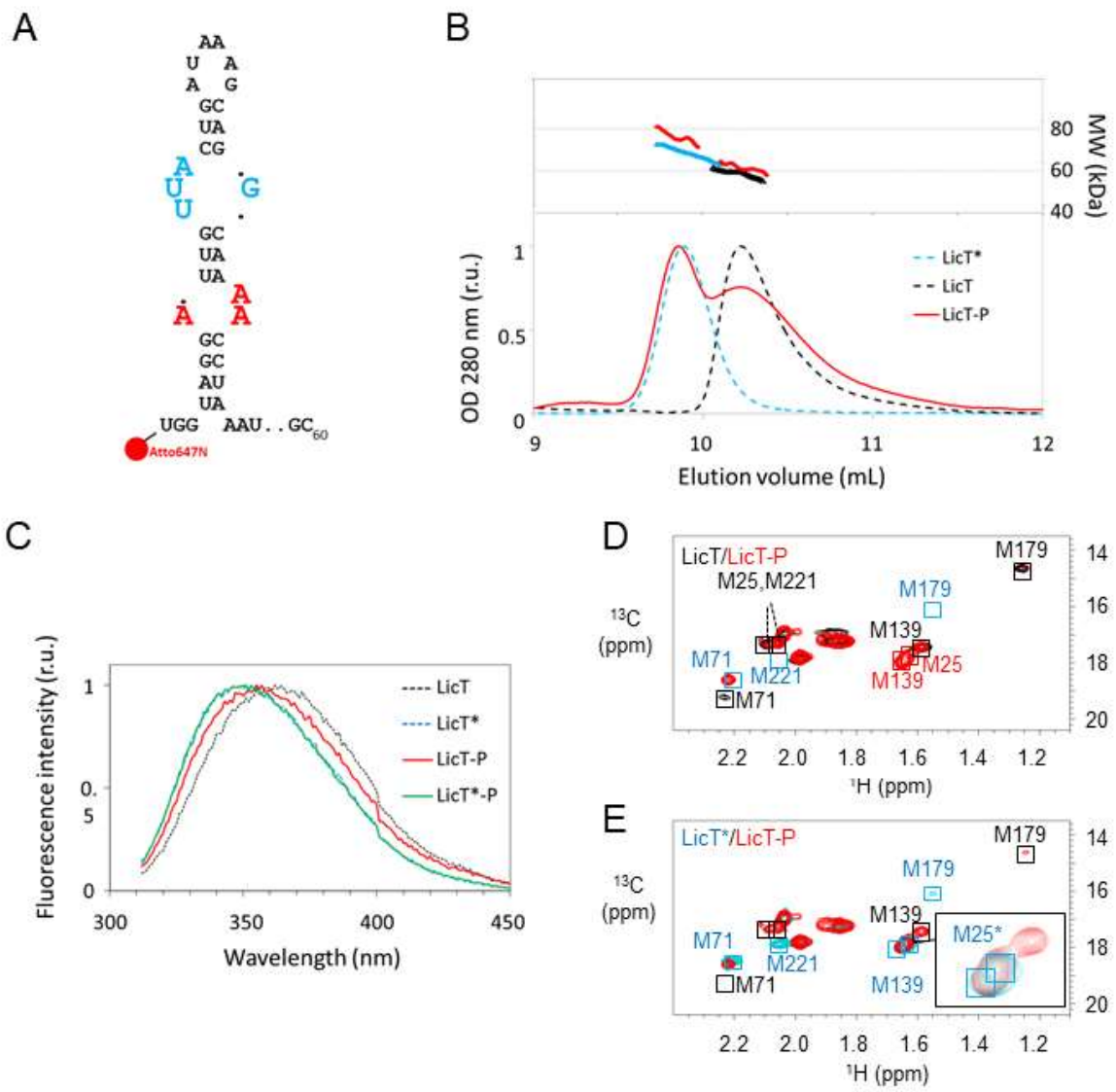

Figure S4, related to Figure3

Figure S4. Characterization of LicT activity and conformation upon phosphorylation (related to Figure 3).

(A) Schematics of the licS-RAT RNA hairpin used for fluorescence anisotropy experiments. The position of the Atto647N label is indicated by a red circle.

(B) Combined size exclusion chromatography (SEC) and multi-angle light scattering (MALS) analysis of the normalized elution profiles shown in Figure 3B for native LicT and activated mutant LicT* (dotted black and blue curves), and for native LicT after incubation with the PTS enzymes and removal of the phosphorylating enzymes by gel filtration (LicT-P, red curve). The upper panel shows the estimated molecular masses of eluted molecules.

(C) The superposition of fluorescence emission spectra of LicT, LicT*, LicT-P and LicT*-P shows that phosphorylation drives the unique Trp residue of LicT in an environment identical to that of activated LicT*.

(D-E) Superposition of ^{1}H-^{13}C HMQC spectra of ^{13}C-CH_3-ε-Met **(D)** LicT (black) and LicT-P (red), **(E)** LicT* (blue) and LicT-P (red). Position of the correlation peaks of the dimeric conformation markers are indicated by blue squares for phosphomimetic LicT* and black squares for native LicT. Two blue squares remain empty (M179 and M221), even at a LicT 300 μM concentration (used here), showing a different dynamical behavior of PRD2 module between phosphorylated LicT-P and mutant activated LicT*. From the analysis of M139 shift, the phosphorylation level was estimated to reach 80% and 40% at a LicT/HPr/EI ratios of 4/0.6/2 (Figure 3) and 4/0.2/0.5 (this figure, insert) respectively.